Cancer Cell
Article

Mutant p53 Prolongs NF-κB Activation and Promotes Chronic Inflammation and Inflammation-Associated Colorectal Cancer

Tomer Cooks,[1] Ioannis S. Pateras,[2] Ohad Tarcic,[1] Hilla Solomon,[1] Aaron J. Schetter,[3] Sylvia Wilder,[1] Guillermina Lozano,[4] Eli Pikarsky,[5,6] Tim Forshew,[7] Nitzan Rozenfeld,[7] Noam Harpaz,[8] Steven Itzkowitz,[9] Curtis C. Harris,[3] Varda Rotter,[1] Vassilis G. Gorgoulis,[2,10] and Moshe Oren[1,*]

[1]Department of Molecular Cell Biology, Weizmann Institute of Science, Rehovot 76100, Israel
[2]Molecular Carcinogenesis Group, Department of Histology-Embryology, School of Medicine, University of Athens, 15771 Athens, Greece
[3]Laboratory of Human Carcinogenesis, National Cancer Institute, National Institutes of Health, Bethesda, MD 20892, USA
[4]Department of Genetics, The University of Texas MD Anderson Cancer Center, Houston, TX 77030, USA
[5]Department of Immunology and Cancer Research
[6]Department of Pathology
Hebrew University Hadassah Medical School, Jerusalem 91120, Israel
[7]Cancer Research UK Cambridge Institute, University of Cambridge, Li Ka Shing Centre, Cambridge CB2 0RE, UK
[8]Department of Pathology
[9]Division of Gastroenterology, Department of Medicine
Mount Sinai School of Medicine, New York, NY 10029, USA
[10]Biomedical Research Foundation, Academy of Athens, 11527 Athens, Greece
*Correspondence: moshe.oren@weizmann.ac.il
http://dx.doi.org/10.1016/j.ccr.2013.03.022

SUMMARY

The tumor suppressor p53 is frequently mutated in human cancer. Common mutant p53 (mutp53) isoforms can actively promote cancer through gain-of-function (GOF) mechanisms. We report that mutp53 prolongs TNF-α-induced NF-κB activation in cultured cells and intestinal organoid cultures. Remarkably, when exposed to dextran sulfate sodium, mice harboring a germline p53 mutation develop severe chronic inflammation and persistent tissue damage, and are highly prone to inflammation-associated colon cancer. This mutp53 GOF is manifested by rapid onset of flat dysplastic lesions that progress to invasive carcinoma with mutp53 accumulation and augmented NF-κB activation, faithfully recapitulating features frequently observed in human colitis-associated colorectal cancer (CAC). These findings might explain the early appearance of p53 mutations in human CAC.

INTRODUCTION

The connection between inflammation and cancer has drawn intensive research (Ben-Neriah and Karin, 2011; Demaria et al., 2010; Hanahan and Weinberg, 2011; Schetter et al., 2010), and has highlighted the context-dependent modulation of inflammation-associated cancer by the transcription factor NF-κB (Ben-Neriah and Karin, 2011; He and Karin, 2011). One well-documented link between chronic inflammation and human cancer involves colorectal cancer (CRC) in patients suffering from inflammatory bowel disease (IBD) (Asquith and Powrie, 2010; Ullman and Itzkowitz, 2011). Continuous tissue destruction and renewal, together with persistent oxidative damage inflicted by the inflamed microenvironment, can trigger mutagenic processes that serve as cancer-initiating events. Further tumor progression is augmented by the continuous presence

Significance

The links between chronic inflammation and cancer are the subject of extensive research. Identification of the underlying molecular mechanisms may be of high relevance for cancer prevention and treatment. Here, we demonstrate that a cancer-associated mutant isoform of the p53 tumor suppressor promotes chronic inflammation and inflammation-driven cancer. Specifically, we report that mutant p53 acquires a significant proinflammatory activity mediated by NF-κB, which may promote both tumor initiation and tumor progression. Furthermore, we describe a mouse model that faithfully mimics features frequently seen in human colitis-associated colorectal cancer. As p53 mutations occur very early in the course of inflammation-associated human colorectal cancer, targeting those mutations in premalignant lesions may be clinically beneficial.

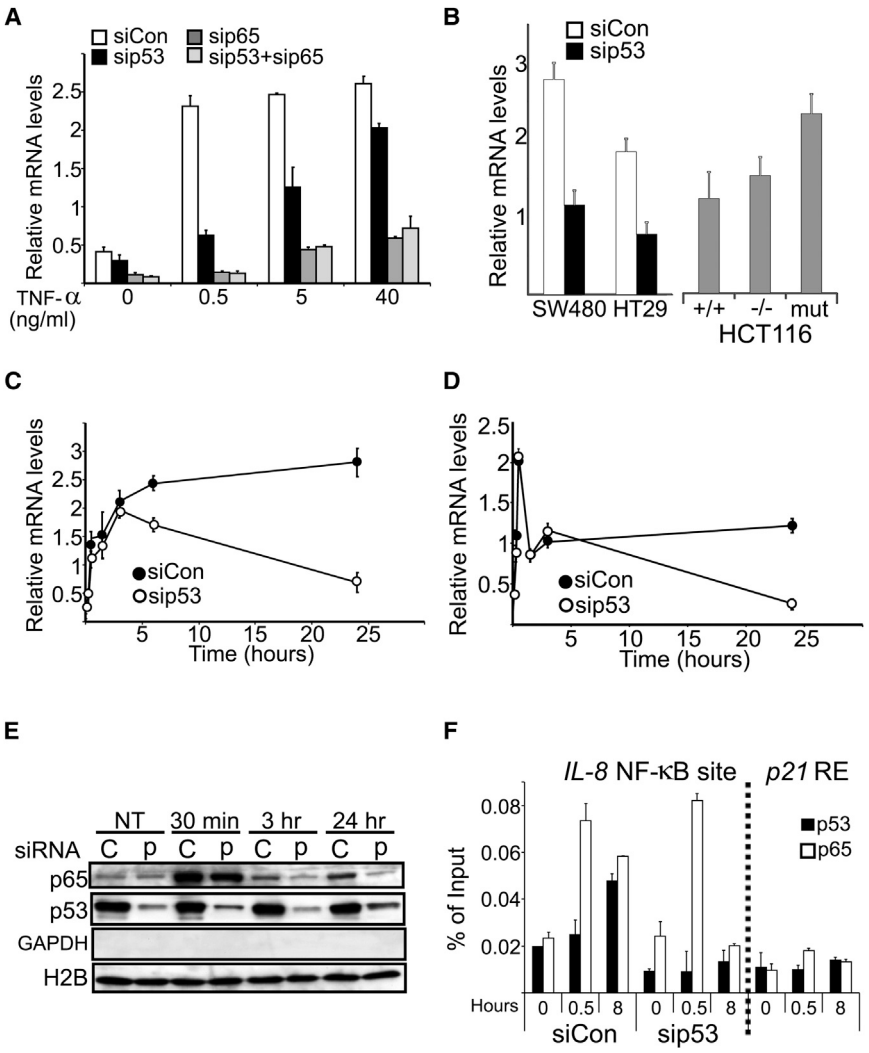

Figure 1. Mutp53 Prolongs TNF-α-Induced NF-κB Activation

(A) PANC-1 cells were transfected with siRNA oligonucleotides specific for p53 (sip53) or lacZ as control (siCon). Forty-eight hours later, TNF-α was added at the indicated final concentrations for an additional 24 hr. RNA was extracted and subjected to qRT-PCR analysis with primers specific for *IL-8* mRNA. Values were normalized for *GAPDH* mRNA in the same sample.

(B) SW480, HT29, HCT116 (+/+), and HCT116 derivatives without p53 (−/−) or with a knockin p53R248W (mut) were transfected as in (A) and exposed to 0.5 ng/ml TNF-α for 24 hr. *IL-8* mRNA was quantified as in (A).

(C) PANC-1 cells were transfected as in (A) and exposed to 0.5 ng/ml TNF-α for the indicated periods. RNA was extracted and subjected to qRT-PCR analysis with primers specific for *IL-8* mRNA. Values were normalized as in (A).

(D) The same RNA samples as in (B) were subjected to qRT-PCR analysis with primers derived from the first intron of the *IL-8* gene. Values were normalized as in (A).

(E) PANC-1 cells were transfected with siRNA oligonucleotides specific for p53 (p) or scrambled oligonucleotides as control (C), treated with 0.5 ng/ml TNF-α for the indicated time periods, and harvested. Chromatin-bound proteins (see Experimental Procedures) were subjected to western blot analysis with the indicated antibodies. GAPDH and H2B served to assess the absence of cytoplasmic contamination and the presence of chromatin, respectively. NT, non-treated.

(F) PANC-1 cells were treated with TNF-α (0.5 ng/ml) for 0, 0.5, or 8 hr and subjected to ChIP with p65 and p53 antibodies, followed by qPCR analysis with primers flanking the NF-κB site of the *IL-8* promoter or the upstream p53-responsive element (RE) of the *p21* gene (negative control). Values are presented as percentage of input. Error bars represent ± SD. See also Figure S1.

of inflammatory cytokines, which may promote excessive cell proliferation and survival through activation of NF-κB and additional signaling pathways.

The p53 tumor suppressor provides powerful intrinsic defense against cancer (Levine and Oren, 2009; Vousden and Prives, 2009). Mutations in the *TP53* gene are the most frequent genetic alteration in human cancer. The main selective advantage of such mutations is through abrogation of wild-type (WT) p53-mediated tumor suppression. Yet, at least some frequently observed p53 mutations also contribute actively to cancer development through gain-of-function (GOF) activities (Brosh and Rotter, 2009; Oren and Rotter, 2010; Rivlin et al., 2011). This may involve enhancement of invasive properties, attenuation of apoptosis, and increased genomic instability. Of note, mutant p53 (mutp53) has been reported to augment NF-κB activation in cultured cells presumably through direct protein-protein interaction (Schneider et al., 2010; Scian et al., 2005; Weisz et al., 2007). Because NF-κB is a master regulator of inflammation and a modulator of inflammation-associated cancer, it is plausible that mutp53 GOF may also impact the latter processes.

In the present study, we investigated the conjecture that mutp53 may promote chronic inflammation and inflammation-associated cancer.

RESULTS

Mutp53 Prolongs NF-κB Activation by TNF-α

We explored mutp53 GOF activity employing the human pancreatic cancer-derived PANC-1 cell line, which harbors the p53R273H mutant. NF-κB activation was triggered by TNF-α; however, in addition to the usual high concentrations for short durations, we also included longer exposures to lower concentrations to mimic a chronic inflammatory state. Remarkably, siRNA-mediated transient depletion of mutp53 (Figure S1A available online) strongly attenuated the induction of *IL-8*, a prototypic NF-κB target gene, by low (0.5 ng/ml) TNF-α concentrations (Figure 1A, compare sip53 to siCon). This was reproduced with different p53 siRNA oligos and shRNA-mediated stable mutp53 knockdown (Figure S1B), making this being an off-target effect unlikely. Knockdown of the p65 NF-κB subunit

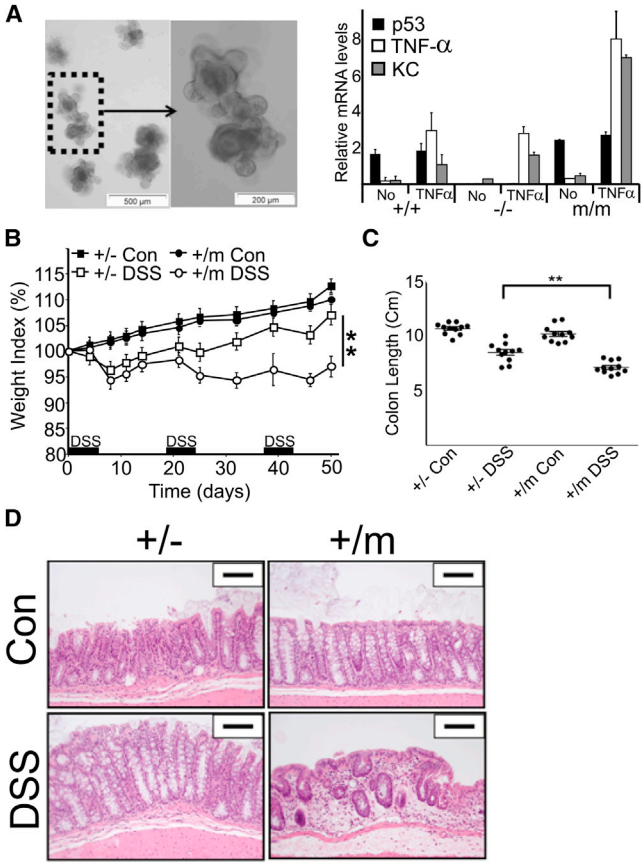

Figure 2. Mice Expressing Mutp53 Are Excessively Susceptible to DSS

(A) Organoids composed of intestinal epithelial cells of $p53^{+/+}$, $p53^{-/-}$, and $p53^{m/m}$ mice were cultured as in Experimental Procedures. Left: representative photomicrograph at both low magnification (scale bar represents 500 μm) and higher magnification (scale bar represents 200 μm). Right: they were then treated with TNF-α (0.5 ng/ml) for 24 hr. *p53*, TNF-α, and KC mRNA levels were quantified as in Figure 1A. Bars represent ± SD.

(B) $p53^{+/-}$ and $p53^{+/m}$ mice were treated with 2% DSS at the indicated time windows or left untreated (Con). Body weight was monitored throughout the indicated period. Values represent average relative weight normalized to the weight at the start of the treatment. Bars indicate standard errors. $^{**}p < 0.01$.

(C) $p53^{+/-}$ and $p53^{+/m}$ mice were treated as in (B). Mice were sacrificed at day 50 and colon lengths were measured. Distributions of individual measurements along with mean and standard deviation are shown. $^{**}p < 0.01$.

(D) Colons of $p53^{+/-}$ and $p53^{+/m}$ mice, either untreated (Con) or treated with DSS, were collected at day 60 and subjected to histopathological analysis (scale bars represent 100 μm).

See also Figure S2.

confirmed that induction was NF-κB dependent (Figure 1A, sip65). Additional NF-κB targets were similarly affected by mutp53 depletion (Figure S1C). Interestingly, mutp53 dependence was most pronounced at low TNF-α concentrations (Figure 1A). Mutp53 depletion had no further effect in the absence of p65 (sip53+sip65), supporting an epistatic interaction wherein mutp53 boosts *IL-8* expression via p65/NF-κB. Similar effects of mutp53 depletion were observed in CRC-derived SW480 and HT29 cell lines (Figure 1B). Conversely, CRC-derived HCT116 cells expressing only mutp53 (Figure 1B, mut) (Sur et al., 2009) displayed elevated *IL-8* induction relative to their WT p53 (+/+) or p53 knockout (−/−) counterparts.

Kinetic analysis of *IL-8* mRNA induction by low (0.5 ng/ml) TNF-α revealed that mutp53 was dispensable for the rapid early rise in *IL-8* mRNA (Figure 1C). However, whereas in control PANC-1 cells (siCon) high *IL-8* mRNA persisted for many hours, mutp53 depletion severely shortened the response duration. Hence, mutp53 prolongs the NF-κB response to limiting amounts of inflammatory cytokine, converting it from transient into chronic. Consistent with earlier observations (Schneider et al., 2010; Weisz et al., 2007), experiments employing a luciferase reporter under an NF-κB-regulated promoter (Figure S1D) confirmed a transcriptional mechanism. This was validated by quantitative (q)RT-PCR analysis of *IL-8* pre-mRNA using intron-derived primers (Kuroda et al., 2005; Phelps et al., 2006; Shema et al., 2008) (Figure 1D). Remarkably, this revealed a biphasic transcriptional response, where the first rapid phase was indifferent to mutp53, whereas the second, later phase was highly dependent on mutp53. Thus, *IL-8* transcription reverted to basal levels by 24 hr in mutp53-depleted cells but continued unabated in mutp53-expressing cells. Notably, augmented association of p65 with chromatin, peaking at 30 min, remained detectable at 24 hr in mutp53-expressing (Figure 1E, C lanes) but not mutp53-depleted cells (p lanes), probably underpinning the extended transcriptional response. Although mutp53 binds many NF-κB sites (Dell'Orso et al., 2011), global association of mutp53 with chromatin was unaltered (Figure 1E). However, chromatin immunoprecipitation (ChIP) analysis revealed recruitment of both p65 and mutp53 to the NF-κB site of the *IL-8* promoter (Figure 1F). Remarkably, mutp53 depletion resulted in complete loss of p65 occupancy by 8 hr. Prolonged p65 retention coincided with enhanced recruitment of mutp53; this suggests a crucial role for mutp53 in maintaining NF-κB chromatin association, consistent with data obtained using DNA oligonucleotides (Schneider et al., 2010). To further characterize the impact of mutp53, we performed expression microarray analysis on control and mutp53-depleted PANC-1 cells, with or without TNF-α (Gene Expression Omnibus [GEO] accession number GSE43738). Indeed, induction of numerous genes by TNF-α was significantly attenuated by mutp53 knockdown (Figure S1E).

To determine whether our findings apply also to nontransformed epithelial cells, 3D intestinal organoid cultures (Sato et al., 2009) (Figure 2A, left) were prepared from $p53^{515A}$ "knockin" mice carrying a germline mutp53 allele encoding p53R172H, the mouse equivalent of the human hot spot mutant p53R175H (Lang et al., 2004), as well as from WT (+/+) and p53 knockout (−/−) mice. These organoids, composed purely of epithelial cells, were then challenged with 0.5 ng/ml TNF-α for 24 hr. Remarkably, the presence of mutp53 greatly augmented the expression of KC (a mouse functional homolog of IL-8) and TNF-α mRNA (Figure 2A, right), confirming the trend seen in human cancer cells.

A similar pattern was observed when comparing mouse embryonic fibroblasts (MEFs) of different genotypes: WT (+/+), p53 knockout (−/−), and homozygous (m/m) or heterozygous (+/m) for the $p53^{515A}$ allele (Figure S2A). Following exposure to 1 or 20 ng/ml TNF-α, induction of KC mRNA was strongly

enhanced and prolonged in +/m and m/m MEFs. Transient p65 knockdown confirmed that this was largely NF-κB dependent (Figure S2B). Hence, a single mutp53 allele suffices for robust prolongation of the NF-κB response. This did not occur in $p53^{-/-}$ MEFs, clearly demonstrating a mutp53 GOF effect. Additional NF-κB-regulated cytokine genes displayed a similar trend (Figure S2C). Likewise, primary mouse monocytes displayed a robust mutp53-mediated increase in the amount of KC protein secreted upon TNF-α stimulation (Figure S2D).

Thus, in both epithelial and nonepithelial cells, mutp53 enforces an extended NF-κB response to an otherwise self-limiting proinflammatory trigger.

Mice Expressing Mutp53 Are Excessively Susceptible to Chronic Inflammation and Tissue Damage

The ability of mutp53 to establish a "chronic" state of NF-κB activation in cultured cells raised the question of whether mutp53 might also promote chronic inflammation and inflammation-associated carcinogenesis in vivo. To address these possibilities, $p53^{515A}$ mice were utilized. Of relevance, p53R175H mutations have been detected in neoplastic and preneoplastic lesions of colitis patients (Leedham et al., 2009; Noffsinger et al., 2001). Repeated exposure of mice to the inflammation-inducing agent dextran sodium sulfate (DSS) elicits a condition resembling human IBD, including late-onset colorectal tumors (Clapper et al., 2007). We employed DSS either in a chronic setting, involving three intermittent cycles of DSS over a total period of 43 days, or an acute setting, involving a single 7 day treatment (Figure S2E; all subsequent numbering relates to day 0).

Homozygous mutp53 mice are highly prone to early-onset spontaneous cancer (Lang et al., 2004; Lozano, 2010; Olive et al., 2004). Given the relatively long duration of the standard DSS carcinogenesis protocol and the ability of a single mutp53 allele to induce a prolonged NF-κB response in primary mouse cells (Figures S2A and S2D), we therefore opted to use heterozygous mutp53 mice, whose spontaneous tumors emerge relatively late (Lang et al., 2004; Olive et al., 2004). Specifically, we compared mice carrying a single mutp53 allele (+/m) or a single p53 knockout allele (+/−).

Exposure to DSS inflicts damage to the distal colon, with consequent weight loss. The two genotypes were similarly affected by the first DSS cycle, exhibiting comparable weight loss (Figure 2B). However, upon repeated DSS treatments, a marked difference became apparent: whereas +/− mice recovered fairly well, +/m mice progressively lost weight, suggesting sustained tissue damage. Indeed, determination of colon length at day 50 revealed more severe shortening of the colon in +/m as compared to +/− mice (Figure 2C). Histological examination confirmed chronic tissue damage in +/m colons, including loss of glands, glandular architectural distortion, and extensive edema and inflammatory infiltrates (Figure 2D), whereas +/− colons appeared to be undergoing effective tissue repair. This was confirmed by quantitative analysis of crypt loss (Malaterre et al., 2007) (Figure S2F). Notably, mutp53 did not significantly affect intestinal barrier function following either acute or chronic DSS treatment (Figure S2G). Thus, mutp53 hampers tissue recovery and renders mice more susceptible to the deleterious effects of DSS.

The ability of mutp53 to prolong the expression of proinflammatory genes, together with the exacerbated response of +/m mice to DSS, suggested that these mice were experiencing accentuated chronic inflammation. This was directly confirmed by endoscopy (Figure 3A). Unlike +/− colons, +/m colons revealed ample evidence of active inflammation, including diffuse mucosal erythema and edema with disappearance of mucosal vessels and shallow ulcers. Systematic endoscopic follow-up, applying a semiquantitative inflammatory score (see Experimental Procedures), revealed that whereas inflammation was similarly induced in both genotypes at early times (Figure 3B), inflammation was attenuated in +/− colons, with most areas regaining near-normal morphology, but persisted in +/m colons (Figure 3C). Hematoxylin-eosin staining confirmed massive presence of both active and chronic constituents of inflammation in +/m colons (Figure 3D), including lymphoplasmacytic aggregates and neutrophils infiltrating the cryptic epithelium and forming crypt abscesses (grade 5). This was much milder in +/− colons (grade 2). Severity of colitis was graded as described in Geboes et al. (2000), evaluating structural change, chronic inflammation, lamina propria neutrophils, neutrophils in epithelium, crypt destruction, and erosions or ulcers.

Quantification of secreted proinflammatory cytokines in the colon (Figure 3E; Figures S3A and S3B) revealed that both genotypes mounted an abundant cytokine response at very early times, which subsided gradually in +/− but remained chronically elevated in +/m mice. To assess the involvement of the colonic epithelial cells in this response, epithelial cell-enriched (ECE) fractions prepared from colons of both genotypes were subjected to RNA analysis. Relative to +/− ECE, +/m ECE expressed significantly higher levels of several proinflammatory cytokine mRNAs (Figure 3F), implying augmented NF-κB activation. Unexpectedly, p65 mRNA levels were also higher in the +/m ECE, although p65 protein levels were not significantly elevated (data not shown).

Thus, mice harboring a germline mutp53 allele display a markedly enhanced propensity for chronic inflammation and failure to resolve inflammation-associated tissue damage. The mice employed here carry mutp53 in all their cells. This might augment NF-κB activation not only in the epithelium but also in other tissues, including the myeloid compartment, as suggested by Figure S2D. To evaluate the relative contribution of different tissue compartments to mutp53-driven chronic inflammation, we generated bone marrow chimeras. Briefly, irradiated +/− and +/m mice were reconstituted with bone marrow from nonirradiated animals of either genotype and subjected to chronic DSS treatment. Regardless of donor and recipient genotype, mixed chimeras underwent substantial weight loss, albeit less pronounced than when both donor and recipient were +/m (Figure S3C). However, good recovery was achieved when both donor and recipient were +/−. Concurrently, both types of mixed chimera displayed elevated chronic inflammation (Figures S3D and S3E). Hence, augmented chronic inflammation is driven by mutp53 GOF in multiple body compartments, probably entailing a mutually reinforcing cytokine-mediated crosstalk between the colonic epithelium and myeloid as well as other stromal cells.

Mutp53 exerts an unequivocal GOF effect on the proinflammatory transcriptional response in cultured mouse cells (Figures

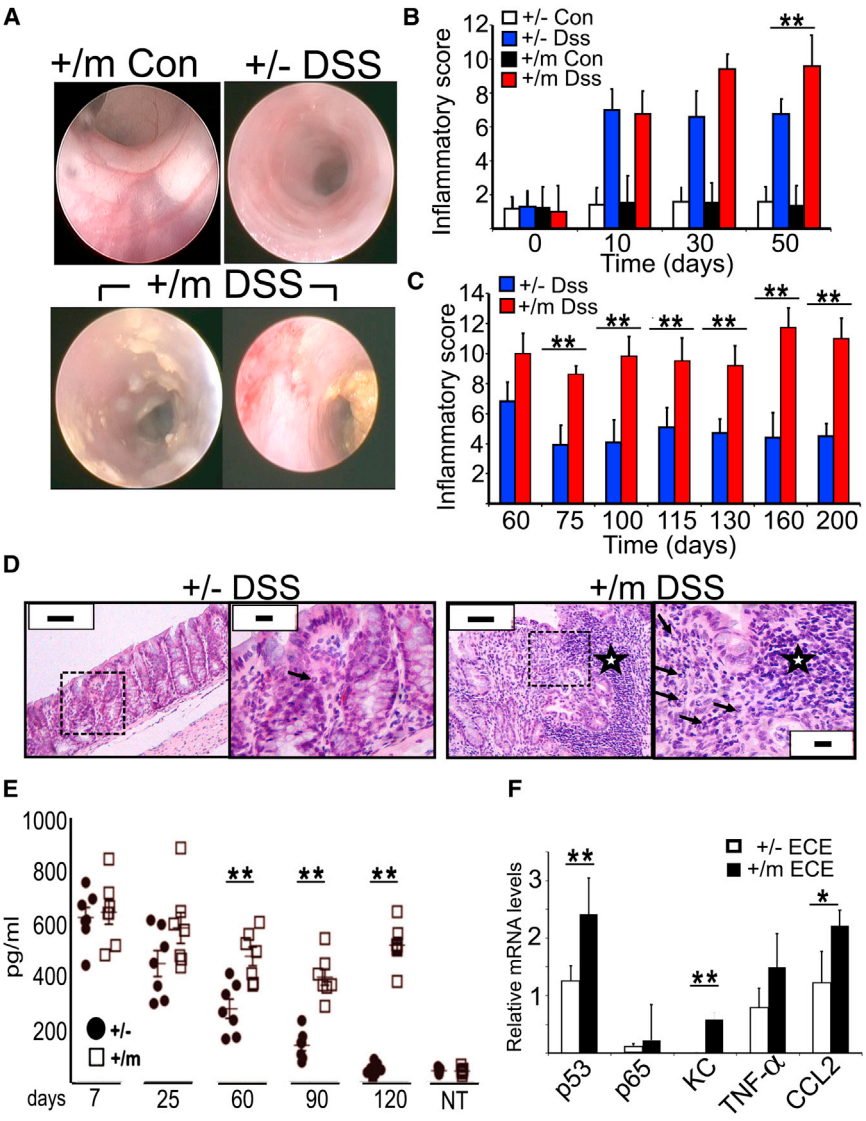

Figure 3. Mice Expressing Mutp53 Are Prone to Chronic Inflammation

(A) Representative colonoscopy images of $p53^{+/-}$ and $p53^{+/m}$ mice subjected to chronic DSS treatment (DSS) or left untreated (Con) at day 50.

(B and C) $p53^{+/-}$ and $p53^{+/m}$ mice, treated as in (A), were subjected to colonoscopy at the indicated time points and scored blindly. An average inflammatory score was calculated (n = 5 mice/group). $^{**}p < 0.01$.

(D) Histopathological analysis of mouse colon sections at day 107. Low (scale bars represent 200 μm) and high (scale bars represent 50 μm) magnifications are shown for each specimen; dashed rectangles indicate the enlarged areas. Asterisks indicate lymphocytic aggregations; arrows indicate neutrophils. Note the existence of an area with microerosion in the +/m DSS case.

(E) Colons were obtained from DSS-treated mice at the indicated time points, and levels of secreted TNF-α were assessed as described in Experimental Procedures. Distributions of individual mice together with mean plus standard deviation for each group are shown. NT, nontreated. $^{**}p < 0.01$.

(F) Epithelial cell-enriched fractions were obtained from DSS-treated mice at day 60. RNA was extracted and subjected to qRT-PCR with primers specific to the indicated genes. Values were normalized to *GAPDH* mRNA in the same sample. $^{*}p < 0.05$; $^{**}p < 0.01$.

Error bars represent ± SD. See also Figure S3.

S2A–S2D). Yet, one could still argue that the in vivo effects are not due to true GOF but rather to a dominant-negative mechanism, wherein the p53R172H protein inactivates the remaining WT p53 protein in the +/m mice and contributes to chronic inflammation merely by rendering the cells practically devoid of WT p53 activity. We therefore compared the DSS response of homozygous $p53^{-/-}$ and $p53^{m/m}$ mice. Remarkably, weight loss in −/− mice was very similar to +/− and WT mice (Figure 4A), arguing that loss of WT p53 function does not explain the exaggerated DSS hypersensitivity. In stark contrast, +/m mice exhibited enhanced progressive weight loss. Although not statistically significant, this appeared even slightly more severe in m/m mice. The differences between −/− and m/m mice were confirmed by monitoring the inflammatory score (Figure 4B). Thus, also in vivo, mutp53 exerts proinflammatory GOF. Indeed, DSS-treated m/m mice suffered increased mortality (Figure 4C), presumably owing to superimposition of persistent tissue damage on the inherent morbidity of mice lacking WT p53.

Mutp53 Mice Are Highly Prone to DSS-Induced Colon Carcinoma

The propensity of mutp53 mice to perpetuate unresolved chronic colonic inflammation raised the question of whether they are more prone to inflammation-associated CRC. For up to 60 days (18 days after the last DSS cycle), no neoplastic lesions were observed by histopathological examination in the colons of either +/− or +/m mice (Figure 5A). However, by day 75, low-grade dysplastic lesions were discernible in several +/m mice, increasing in number and grade by day 90. By day 100, invasive carcinoma was already apparent in some cases (Figure 5B). Angular irregularly shaped glands of well-differentiated tubuloglandular colorectal adenocarcinoma were observed invading through the muscularis mucosae into the submucosa. By day 120, multifocal adenocarcinoma was seen only in +/m colons, with abundant extracellular mucin production, reminiscent of human mucinous colorectal adenocarcinoma. The cancerous glands penetrated the submucosa, accompanied by desmoplastic reaction of the surrounding stroma. The overlying epithelium was dysplastic, encompassing areas with low- and high-grade flat dysplasia (Figure 5C). Invasion through the muscularis mucosae was confirmed by smooth muscle actin (SMA) immunostaining (Figure 5B). Flat dysplastic lesions are hard to detect by standard colonoscopy, particularly at early stages; however, at later time points, suspicious dysplasia-associated

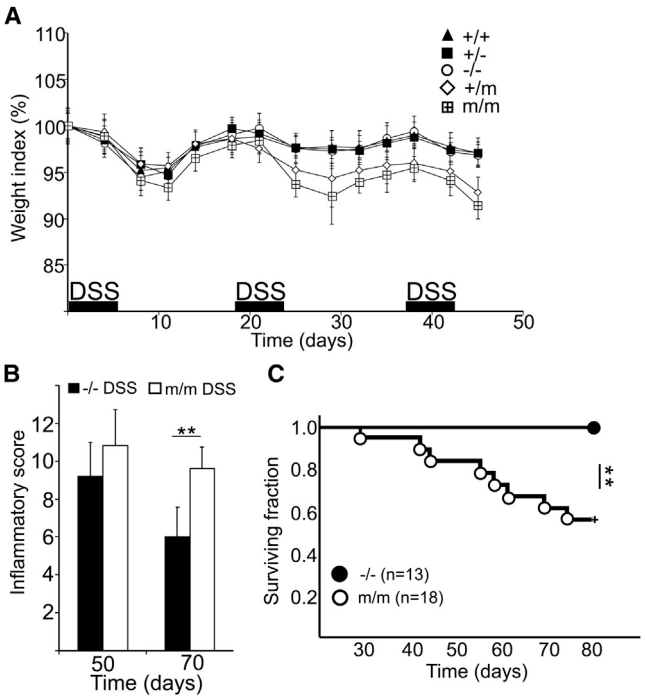

Figure 4. Gain-of-Function Effect of Mutp53

(A) Mice of the indicated genotypes were treated and analyzed as in Figure 2B. Only DSS-treated mice are shown. Error bars represent ± SE.

(B) $p53^{-/-}$ and $p53^{m/m}$ mice were treated with DSS as in Figure 2B and monitored periodically by colonoscopy. Inflammatory scores were determined as in Figure 3B. **$p < 0.01$. Error bars represent ± SD.

(C) Kaplan-Meier plot showing survival of DSS-treated $p53^{-/-}$ and $p53^{m/m}$ mice. **$p < 0.01$ by Mantel-Cox test.

lesions or masses were sometimes observed (Figure S4A), confirmed by gross assessment of the colon (Figure S4B) and subsequent histopathological examination, which also revealed the presence of invasive carcinoma with extracellular mucin production (Figures S4C and S4D). Throughout that entire period, no neoplastic lesions were detected in any +/− mouse. As expected, chronic inflammation was suppressed by treatment of +/m mice with the anti-inflammatory drug sulindac, initiated 7 days after the last DSS cycle (Figures S4E and S4F). Importantly, sulindac inhibited DSS-induced carcinogenesis (Figures S4G and S4H), confirming that this mutp53 GOF effect relies on its ability to elicit chronic inflammation. Thus, mutp53 not only makes the mice more susceptible to chronic inflammation but also greatly accelerates inflammation-associated colon cancer.

Mutp53 Accumulates in the Inflamed Colon and in Cancerous Glands Concomitantly with NF-κB Activation and Sustained DNA Damage

To interrogate molecular events underpinning the GOF effect of mutp53, chromatin from mouse colons was subjected to ChIP analysis. In colons of untreated mice, very little p65 or p53 associated with the NF-κB site of the *MIP2* gene, regardless of p53 status (Figure 6A). After a 7 day acute DSS treatment, p65 occupancy increased considerably in both +/− and +/m colons. Importantly, by day 60 of chronic DSS treatment, p65 remained markedly associated with the NF-κB site only in +/m but not +/− colons, as seen also with several additional genes (Figure S5A). Remarkably, mutp53 was recruited to the same genomic region upon DSS treatment, persisting through day 60. This suggests that in the colon, like in cultured cells (Figures 1E and 1F), mutp53 retains p65 on the chromatin for extended periods.

In colonic epithelium of untreated WT p53 mice, p53 staining was practically undetectable by immunohistochemistry (IHC) (Figure 6B), whereas some p53-positive nuclei were present in +/m and m/m mice, particularly within the lower part of the crypt. Acute 7 day DSS treatment of WT mice triggered modest nuclear p53 accumulation in some cells (Figure 6B). Notably, this was greatly augmented in +/m mice, and even more in m/m ones. This p53 accumulation was likely driven by reactive oxygen and nitrogen species (ROS and RNS) in the inflamed microenvironment (reviewed by Schetter et al., 2010; Ullman and Itzkowitz, 2011). Indeed, expression of inducible nitric oxide synthase (iNOS) was most pronounced in m/m mice and least in +/+ ones, with +/m mice exhibiting variable intermediate iNOS levels (Figure 6C). A similar pattern, consistent with the differential regulation of iNOS expression by WT p53 versus mutp53 (Forrester et al., 1996), also persisted after cessation of DSS treatment in the chronic protocol (Figure S5B). As expected, induction of p53 in WT colons was accompanied by upregulation of p21, a prototypical WT p53 transcriptional target (Figures S5C and S5D, +/+). In contrast, p21 was hardly detected in $p53^{m/m}$ colons, confirming that the mutant p53 was transcriptionally inactive.

Intense mutp53 staining persisted throughout the tumor progression sequence. It was particularly prominent in invasive fronts of cancerous glands (Figure 6D), suggesting that in addition to cell-autonomous factors, local microenvironmental cues may also drive persistent mutp53 stabilization. Furthermore, the strongest mutp53 staining coincided with intense nuclear p65 staining (Figure 6D). This implies that, like in cultured cells, high mutp53 levels may fuel an augmented and prolonged NF-κB response in the colonic epithelium. Interestingly, many of those cells were also positive for phosphorylated histone H2AX (γH2AX; Figure 6D), indicative of persistent DNA damage. This could simply reflect the DNA damage constantly inflicted on the cells within the chronic inflammatory microenvironment. Alternatively, and not mutually exclusive, defective DNA repair in the mutp53 cells might lead to gradual accumulation of unrepaired double-strand breaks and other types of damage. Either way, such exacerbated damage may increase genomic instability, driving the neoplastic lesions toward higher malignancy.

Mutp53 Accumulation Correlates with NF-κB Activation in Human Colitis-Associated Cancer and Nonneoplastic Glands

Human colitis-associated cancer (CAC) involves frequent *TP53* mutations, along with abundant mutp53 protein accumulation in the cancerous glands (reviewed in Asquith and Powrie, 2010; Ullman and Itzkowitz, 2011). To determine whether, like in $p53^{515A}$ mice, this is associated with constitutive NF-κB activation, 18 formalin-fixed, paraffin-embedded CAC specimens from two different sources were subjected to *TP53* tagged-amplicon Illumina HiSeq 2000 sequencing (Forshew et al.,

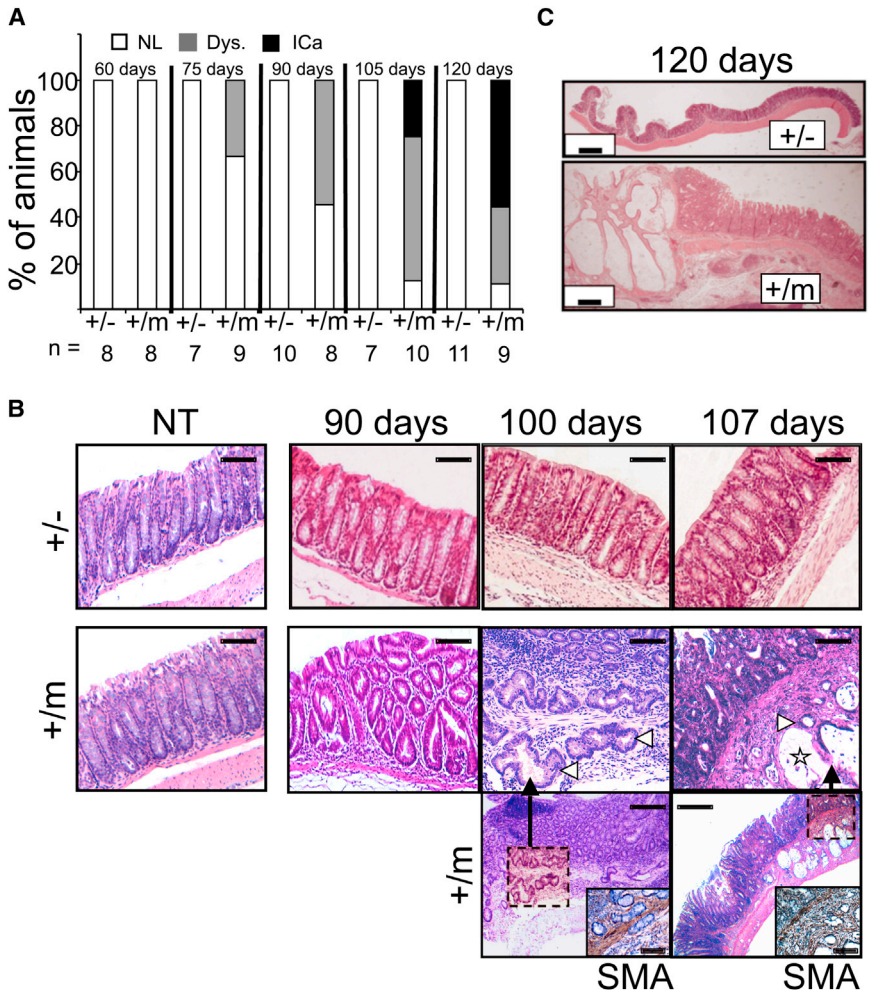

Figure 5. Mutp53 Mice Are Prone to DSS-Induced Colon Carcinoma

(A) $p53^{+/-}$ and $p53^{+/m}$ mice were treated with DSS as in Figure 2B. Mice were sacrificed at the indicated time points and colon sections were subjected to histopathological analysis. Each bar depicts the percentage of mice within a given group scoring positive for the indicated lesions. Numbers of animals/group are noted at the bottom. Dys., dysplasia (low or high grade); ICa, invasive carcinoma; NL, no lesion.

(B) Representative histopathological images of colon sections obtained from nontreated mice (NT) of the indicated genotypes or mice subjected to chronic DSS treatment and sacrificed at the indicated time points. Note the presence of low-grade flat dysplasia in $p53^{+/m}$ cases at 90 days and the development of well-differentiated carcinoma and mucinous adenocarcinoma at days 100 and 107, respectively. Cancerous glands (white arrowheads) invade the muscularis mucosae, identified by SMA staining (insets). The star denotes a pool of extracellular mucin. Scale bars indicate 50 μm (upper), 200 μm (middle), 600 μm (lower), and 100 μm (insets).

(C) Low-magnification images of colon sections from DSS-treated mice of the indicated genotypes, obtained at day 120. Note the progressive multifocal invasive carcinoma with prominent mucin lakes in the $p53^{+/m}$ mouse. Scale bars represent 500 μm.

See also Figure S4.

2012) along with IHC analysis. *TP53* mutations were detected in 16 tumors (Figure S6A). Based on their *TP53* sequence, these tumors were divided into three groups: no p53 mutations (WT p53; 2/18), missense p53 mutations (8/18), and other p53 mutations (nonsense, frameshift, and splicing; 8/18). As expected, intense diffuse nuclear p53 staining was more prominent in the missense mutation cases (Figures 7A and 7B; Figures S6A and S6B). Importantly, consistent with our mouse data, abundant p53 staining correlated strongly with augmented nuclear p65 staining (Pearson correlation coefficient = 0.85), as observed also in head-and-neck cancer and sporadic CRC (Weisz et al., 2007; Schwitalla et al., 2013).

Intense p53 staining in tumors is generally considered indicative of missense mutations; yet, CAC cases with positive p53 IHC but no detectable mutation have been reported (Yoshida et al., 2003). Interestingly, four of our cases carried either the R213X nonsense mutation or the chr17:7578370:C>T splice mutation, both observed repeatedly in human tumors (http://p53.iarc.fr), raising the intriguing possibility that such mutations confer an unexpected GOF. Indeed, in all those four cases, p53 staining was considerably greater than in the remainder "other" mutants (38.1 ± 13.9 average p53 % staining abundance and intensity [%LI] versus 17.8 ± 9.7); this warrants further investigation.

In human CAC, mutp53 accumulation often precedes the appearance of detectable neoplastic lesions (Hussain et al., 2000). To assess whether such early mutp53 accumulation might already drive constitutive NF-κB activation, IHC analysis was performed on specimens from IBD patients experiencing chronic inflammation with no recognizable neoplastic lesions. As exemplified in Figure 7C, the majority of glands displayed relatively weak p53 staining, with occasional areas of stronger positivity (e.g., gland a). Typically, p21 also stained more strongly in the same areas, arguing that the p53-positive cells were expressing WT p53, presumably activated by local stress signals. However, a few glands (exemplified by gland b) exhibited a strikingly different pattern, with strong diffuse nuclear p53 but practically no p21 staining; this was retained also in more lumen-proximal sections of the gland (Figure S6C), suggesting the presence of mutp53 throughout gland b. Remarkably, the same gland also displayed robust NF-κB activation. Dysplasia and cancer can arise from patches of chronically inflamed crypts containing p53 mutations (Leedham et al., 2009); gland b might represent such a mutp53 crypt, potentially serving as a precursor to subsequent neoplasia. Furthermore, as in the mouse, the presence of mutp53 within a chronically inflamed microenvironment appears to kindle persistent NF-κB activation.

In sum, both histologically and molecularly, the $p53^{515A}$ DSS mouse model of IBD-associated cancer closely reproduces features frequently observed in its human counterpart.

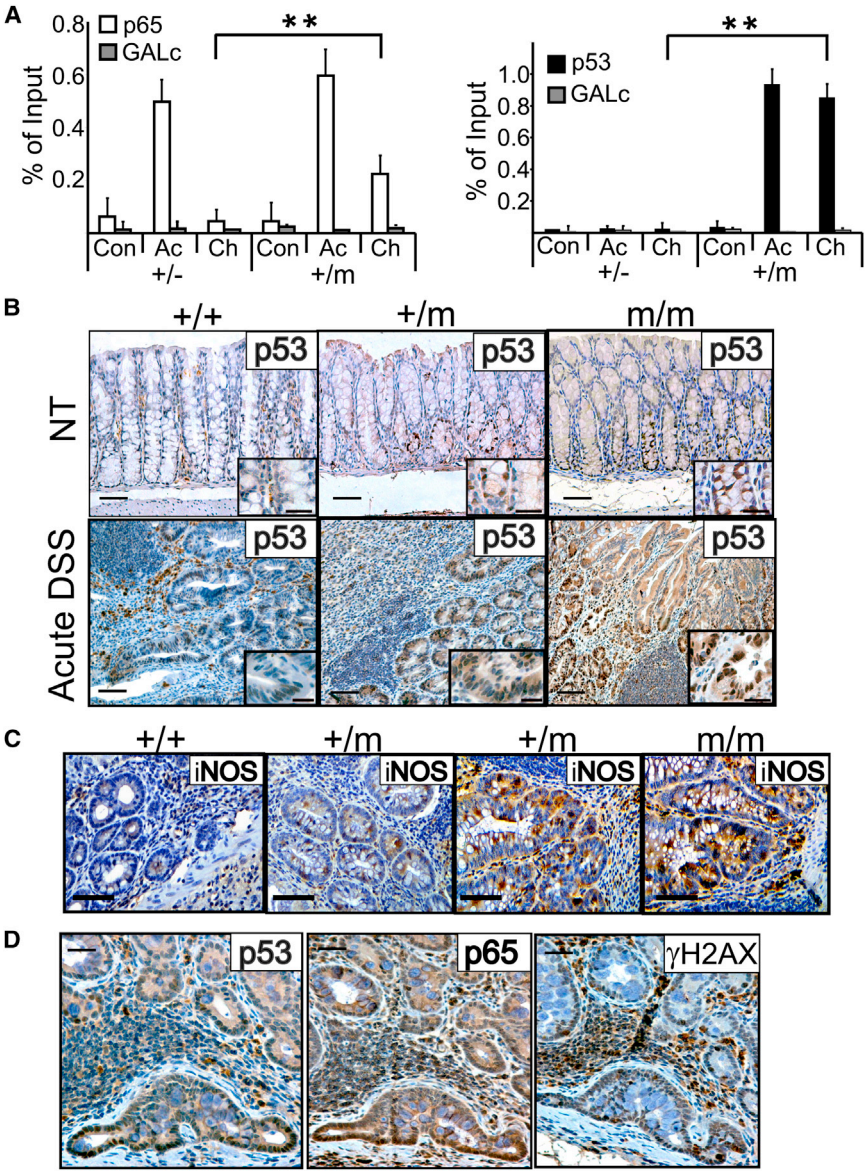

Figure 6. Analysis of p53, p65, iNOS, and γH2AX in DSS-Exposed Mice

(A) Colons of $p53^{+/-}$ and $p53^{+/m}$ mice were harvested without treatment (Con), immediately after acute DSS treatment (Ac), or at day 60 of the chronic DSS protocol (Ch), and subjected to ChIP analysis with antibodies against mouse p65 (left) or mouse p53 (right). Extracted DNA was subjected to qPCR with primers flanking the NF-κB site of the *MIP2* gene promoter. Primers corresponding to a region located far from any coding gene (GALc) served as negative control. ChIP values are presented as percentage of input. $^{**}p < 0.01$.

(B) Colon sections were prepared at day 7 from mice of the indicated genotypes subjected to acute DSS treatment, as well as from nontreated mice (NT), and stained for p53 (scale bars represent 100 μm). Insets display a higher magnification (scale bars in upper insets represent 50 μm and in lower insets represent 25 μm).

(C) Colon sections prepared as in (B) were stained with antibodies against iNOS; sections from two +/m mice are included to show the mouse-to-mouse variability in this genotype. Scale bars represent 50 μm.

(D) Staining for p53, p65, and γH2AX in an invading gland within the colon of a $p53^{+/m}$ mouse, collected at day 105 of the chronic DSS protocol. Scale bars represent 50 μm.

Error bars represent ± SD. See also Figure S5.

Azoxymethane Bypasses the Dependence on Mutp53 GOF for Accelerated Tumorigenesis

In parallel with DSS only, additional +/− and +/m mice were exposed to a standard protocol (Tanaka et al., 2003) combining DSS with the chemical carcinogen azoxymethane (AOM; Figure 8A). As with DSS alone, +/m mice displayed more severe weight loss (Figure 8B). Surprisingly, tumorigenesis was not noticeably accelerated in these mice. Instead, the entire tumor progression pattern was altered, both genotypes rapidly developing massive adenomatous polyps (Figures 8C and 8D) at similar numbers and size (Figure S7A). Remarkably, regardless of genotype, nuclear and cytoplasmic β-catenin accumulation predominated in these tumors (Figures S7B and S7C), consistent with the frequent induction of *Ctnnb* mutations by AOM (Greten et al., 2004) and indicative of robust Wnt pathway activation. In contrast, in DSS-only tumors of +/m mice, β-catenin was retained at the plasma membrane, suggesting the absence of Wnt pathway activation. Notably, whereas Wnt pathway activation is almost unanimous in human sporadic CRC, mostly involving early *adenomatous polyposis coli* (*APC*) mutations, such mutations are typically late and markedly less frequent in human CAC (Ullman and Itzkowitz, 2011). Interestingly, in mice treated with AOM only, where tumor development approximates human sporadic CRC, the mere loss of p53 triggers an inflammatory transcription program and promotes invasiveness (Schwitalla et al., 2013).

Thus, inclusion of a chemical carcinogen switches the response toward a different course with pathological and molecular features commonly observed in sporadic human CRC. In this setting, early p53 mutations do not appear to exert much impact.

DISCUSSION

The course of human IBD-associated neoplasia differs substantially from that of spontaneous CRC. Whereas the latter is characterized by adenomatous polyps, a few percent of which may progress to invasive carcinoma, IBD-associated CRC often involves flat dysplastic lesions that progress from low to high grade and eventually may give rise to invasive carcinoma, although tumor development may skip one of these steps

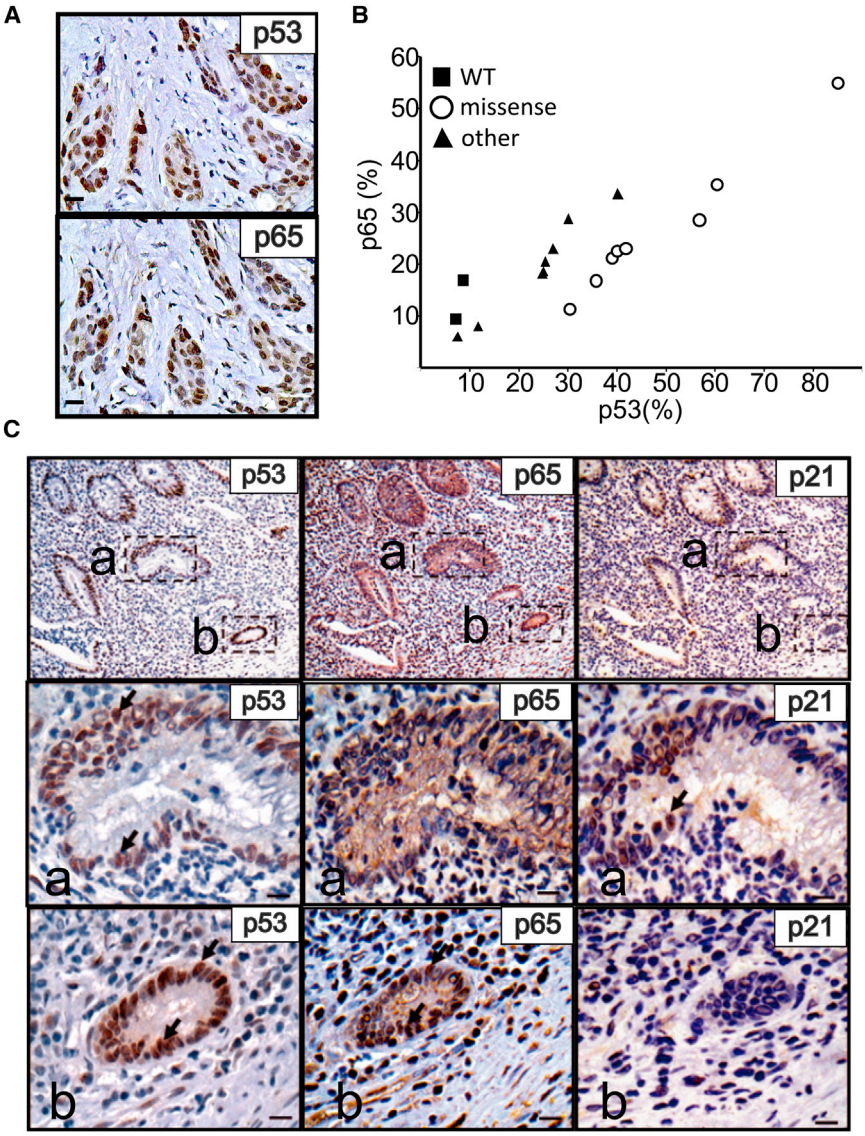

Figure 7. Mutp53-p65 Correlation in Human CAC and IBD

(A) Concurrent strong immunostaining of p53 and nuclear p65 in consecutive serial sections of a representative human CAC case carrying a p53R273H mutation (Figure S6A, case 36102).

(B) Staining abundance and intensity were calculated for all 18 specimens as described in Figure S6A. The scatter plot depicts the p65 and p53 %LI values for each individual tumor. The Pearson correlation coefficient for all groups together is 0.85.

(C) Immunostaining for p53, p65, and p21 in the epithelium, within an area of severe acute inflammation, in a human case of severe active colitis. Upper: a low-magnification field; two glands (a and b) are indicated by dashed rectangles. Higher magnifications of gland a (middle) and gland b (lower) are shown below. Arrows indicate cells with intense nuclear staining. Scale bars represent 50 μm.

See also Figure S6.

(Fearon, 2011; Terzic et al., 2010; Ullman and Itzkowitz, 2011). Likewise, the underlying genetic events also differ. In sporadic CRC, *APC* mutational inactivation is very often the initiating event. In contrast, loss of *APC* function typically occurs late in IBD-associated CRC, in only a minority of tumors. Conversely, even though p53 mutations are highly abundant in both types of CRC, they occur very early in IBD-associated CRC but are considered late events in sporadic CRC (Brentnall et al., 1994; Yin et al., 1993; reviewed in Fearon, 2011; Kinzler and Vogelstein, 1996; Terzic et al., 2010; Ullman and Itzkowitz, 2011). In fact, p53 mutations are enriched in inflamed colonic tissue well before neoplastic lesions become detectable (Hussain et al., 2000). Moreover, analysis of individual crypts suggests that p53 mutations have a founder effect in driving colitis-associated carcinogenesis (Leedham et al., 2009). Thus, p53 mutations probably serve an initiating role in IBD-associated cancer, whereas in sporadic CRC they are more important for transition from localized late adenoma to invasive carcinoma. Yet, in both scenarios, one might argue that p53 mutations serve solely to abrogate the tumor suppressor effects of WT p53, without the need to implicate mutp53 as having GOF.

We now show that mutp53 exerts a distinct GOF activity through augmenting and prolonging the response of epithelial cells to low amounts of inflammatory cytokine, enforcing a chronic state of NF-κB activation. Furthermore, mutp53 instates a chronic inflammatory condition in animals exposed to tissue damage. In the mouse colon, this spawns invasive carcinoma within less than 4 months. These effects, attainable by even a single mutp53 allele, are not reproduced by loss of WT p53.

The greatly accelerated tumorigenesis likely results from a combination of enforced prolonged inflammation associated with persistent tissue damage, increased genome instability, and augmented capacity of mutp53-containing cells to evade apoptosis in the face of the harsh inflammatory microenvironment. These effects may benefit from mutp53's ability to perpetuate NF-κB activation through its prolonged stabilization on κB sites associated with proinflammatory cytokine genes, probably involving physical interactions between mutp53 and NF-κB (Schneider et al., 2010). Notably, the course of disease in mutp53-expressing mice bears striking resemblance to that observed in many cases of human IBD-associated cancer, progressing from low- to high-grade flat dysplasia and finally to invasive carcinoma, without involvement of adenomatous polyps. Our findings support the conjecture that the early presence of p53 mutations in the inflamed colon of IBD patients (Hussain et al., 2000) is not merely a reflection of the mutagenic microenvironment but may actually be a driver of the subsequent emergence of neoplasia by invigorating

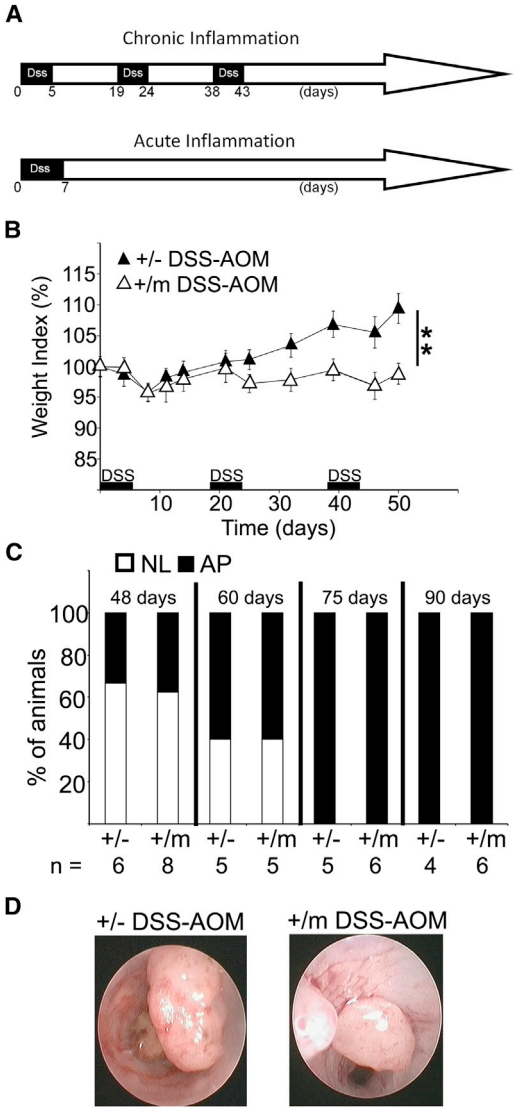

Figure 8. Analysis of Mice Subjected to DSS+AOM

(A) Scheme of treatment schedule with DSS+AOM. $p53^{+/-}$ and $p53^{+/m}$ mice were subjected to treatment with DSS+AOM.

(B) Weight index was monitored and calculated as in Figure 2B. $^{**}p < 0.01$. Error bars represent ± SE.

(C) $p53^{+/-}$ and $p53^{+/m}$ mice treated with DSS+AOM were periodically monitored by colonoscopy. Each bar depicts the percentage of mice within a given group bearing adenomatous polyps (AP) or no lesion (NL); the number of animals/group is indicated at the bottom.

(D) Representative colonoscopy images of polyps in $p53^{+/-}$ and $p53^{+/m}$ mice at day 105 of exposure to the DSS+AOM protocol.

See also Figure S7.

inflammation in the immediate microenvironment of cells harboring mutp53.

Loss of WT p53 can by itself increase DSS-induced tumorigenesis, yielding a mixture of polypoid and flat dysplastic lesions, some of which progress to invasive carcinoma (Chang et al., 2007; Fujii et al., 2004). Hence, WT p53 is a relevant tumor suppressor in this setting. Indeed, numerous studies have revealed an intricate crosstalk between WT p53 and NF-κB, wherein WT p53 often inhibits NF-κB activation but can also sometimes cooperate with NF-κB to orchestrate a more vigorous stress response (Ak and Levine, 2010; Ryan et al., 2000; Tergaonkar and Perkins, 2007; Meylan et al., 2009; Schwitalla et al., 2013). However, in DSS-treated $p53^{-/-}$ mice, cancer develops with long latency (126–160 days) and partial penetrance, even when using high DSS (4%, compared to 2% in our study). By contrast, we show that a single mutp53 allele suffices to elicit a much faster and more aggressive disease course, demonstrating a true GOF effect. Such GOF requires the buildup of high mutp53 concentrations, typically entailing protein stabilization (Brosh and Rotter, 2009; Oren and Rotter, 2010; Rivlin et al., 2011; Suh et al., 2011). Notably, whereas mutp53 accumulation is usually seen in tumors but not in nontransformed mutp53 mouse tissues (Suh et al., 2011; Terzian et al., 2008), we find that under inflammatory conditions this occurs already well before the onset of any observable neoplastic events. This may be due to elevated iNOS expression and higher ROS and RNS (Schetter et al., 2010; Ullman and Itzkowitz, 2011), eliciting genotoxic stress with subsequent p53 stabilization (Suh et al., 2011). A similar mechanism may account for accumulation of mutp53 in seemingly nonneoplastic crypts of human IBD patients, where strong p53 accumulation in the entire crypt suggests that epithelial cells with mutp53 may have gradually taken over the crypt. Repetitive exposure of such a crypt to oxidative stress and inflammatory cytokines, driving constitutive NF-κB activation, probably increases its likelihood to progress toward neoplasia.

Mutp53 GOF effects are particularly prominent in the presence of oncogenic Ras mutations, as demonstrated both in vitro and in vivo (Acin et al., 2011; Buganim et al., 2010; Doyle et al., 2010). Indeed, PANC-1, SW480, and HCT116 cells harbor mutant K-Ras. However, similar effects are observable in HT29 cells, which do not carry Ras mutations. Hence, although Ras mutations may cooperate with mutp53, they are not obligatory for its GOF in augmenting NF-κB activation, as reflected also by the fact that NF-κB activation correlates with mutp53 accumulation in CAC tumors regardless of K-Ras mutations (Figure S6).

The mice employed in this study harbor mutp53 not just in their colonic epithelium but rather in all cell types, including adjacent fibroblasts and mobilized inflammatory cells. Experiments employing intestinal organoids, comprising only epithelial cells, suggest that mutp53-driven augmentation of NF-κB activity may suffice to drive a chronic inflammatory process. Indeed, constitutive activation of NF-κB in the mouse intestinal epithelium is sufficient to establish an inflammatory microenvironment and promote tumorigenesis (Vlantis et al., 2011). However, nonepithelial cells are also prone to mutp53-mediated augmented NF-κB activation. Hence, the accelerated tumorigenesis seen in mutp53 mice may involve a vicious cycle wherein both epithelial and nonepithelial components engage in excessive production of cytokines and an exaggerated response to those cytokines, a conjecture supported by bone marrow chimera experiments. Stromal p53 mutations have been described in several types of human cancer, including CRC (Patocs et al., 2007; Wernert et al., 2001), although this has subsequently been questioned (Campbell et al., 2009). It is plausible that a chronically inflamed microenvironment, characterized by continuous exposure to mutagenic compounds such as ROS

and RNS, could promote stromal p53 mutations, which might potentially contribute to human inflammation-associated cancer. In sum, our findings suggest that by augmenting NF-κB activation, the emergence of p53 mutations in a chronically inflamed microenvironment may both exacerbate the inflammatory response and protect the mutant cells from the deleterious effects of this microenvironment. These GOF effects of mutp53 may account for the apparent early role of p53 mutations in inflammation-associated carcinogenesis.

EXPERIMENTAL PROCEDURES

Cell Culture, Transfection, and Infection

PANC-1 (generous gift of Yoel Kloog), SW480, HT29, and HCT116 cells and their derivatives somatically knocked out for p53 and knocked in for the R248W p53 mutant (Sur et al., 2009) (generous gift of Bert Vogelstein), mouse intestinal organoids, and isolated primary mouse monocytes were maintained at 37°C in a standard 5% CO_2 humidified incubator, whereas mouse embryonic fibroblasts obtained from C57BL/6 mice were maintained at 37°C in a 5% CO_2 and 3% O_2 humidified incubator (Thermo Scientific). Dulbecco's modified Eagle's medium (DMEM) was used for growing PANC-1, SW480, and MEFs, McCoy's medium for HT29 and HCT116 cells, and DMEM/F12 medium for intestinal organoids. DMEM and McCoy's were supplemented with 10% heat-inactivated fetal bovine serum (HI-FBS; Sigma), 2 mM L-glutamine, and antibiotics. Intestinal organoids were cultured in Matrigel with medium containing Glutamax (100×; GIBCO), B27 (1:50; Invitrogen), mouse bFGF (10 ng/ml; Peprotech), human EGF (20 ng/ml; Peprotech), mouse noggin (100 ng/ml; Peprotech), human r-spondin (500 ng/ml; Peprotech), and antibiotics.

For siRNA transfections, Dharmafect 1 reagent (Dharmacon) was used according to the manufacturer's protocol. siRNAs for *p53* and *p65*, as well as control scrambled siRNA, were purchased from Dharmacon as SMARTpools. To exclude off-target effects, ON-TARGET plus p53 siRNA oligos (Dharmacon) were also used (sip53 II; Figure S1B).

For stable clones, ecotropic Phoenix packaging cells were transfected with 10 μg DNA of the appropriate retroviral construct by a standard calcium phosphate procedure. Culture supernatants were collected 36–48 hr after transfection and filtered. PANC-1 cells were infected with the filtered viral supernatants in the presence of 4 μg/ml Polybrene (Sigma) for 12 hr, after which the medium was changed. Fresh viral suspensions were added after a 24 hr interval for an additional 12 hr. Infected cells were selected for 5 days in 2.5 μg/ml puromycin.

Chromatin Immunoprecipitation

Cells were crosslinked with 1% formaldehyde at room temperature for 10 min, washed twice with 10 ml ice-cold PBS, and then scraped into 0.5 ml of lysis buffer (1% SDS, 10 mM EDTA, 50 mM Tris-HCl [pH 8.1], 1 mM PMSF, 1 μg/ml leupeptin, 1 μg/ml aprotinin) and left on ice for 10 min. Samples were then sonicated seven times at 4°C; each sonication was for 20 s, followed by a 40 s pause. Supernatants were recovered by centrifugation at 12,000 rpm in an Eppendorf microfuge for 10 min at 4°C before being diluted 4- to 8-fold in dilution buffer (1% Triton X-100, 2 mM EDTA, 150 mM NaCl, 20 mM Tris-HCl [pH 8.1]). Samples were then precleared for 2 hr at 4°C with 2 μg sheared salmon sperm DNA and 20 μl protein A Sepharose (50% slurry). At this stage, 50 μl of the material was kept as input. Immunoprecipitations were performed overnight with specific antibodies (1–2 μg), with addition of NP-40 to a final concentration of 0.5%. Immune complexes were captured by incubation with 20 μl protein A Sepharose (50% slurry) and 2 μg salmon sperm DNA for 1 hr at 4°C. Immunoprecipitates were washed sequentially for 5 min each at 4°C in TSE 1 (0.1% SDS, 1% Triton X-100, 2 mM EDTA, 20 mM Tris-HCl [pH 8.1], 150 mM NaCl), TSE 2 (0.1% SDS, 1% Triton X-100, 2 mM EDTA, 20 mM Tris-HCl [pH 8.1], 500 mM NaCl), and buffer 3 (0.25 M LiCl, 1% NP-40, 1% deoxycholate, 1 mM EDTA, 10 mM Tris-HCl [pH 8.1]). Beads were washed twice with TE buffer (10 mM Tris-HCl, 1 mM EDTA) and eluted with 500 μl elution buffer (1% SDS, 0.1 M $NaHCO_3$). To reverse the crosslinks, samples were incubated at 65°C overnight, after which DNA was eluted and subjected to qPCR. When mouse colons were subjected to ChIP, epithelium was scraped as described in Guma et al. (2011) and subsequently underwent the same procedure as described above. The primers used for qPCR are listed in Supplemental Experimental Procedures.

RNA and Real-Time Quantitative PCR

RNA was isolated with a NucleoSpin RNA II kit (Macherey-Nagel). Aliquots (1.5 μg) were reverse transcribed using Moloney murine leukemia virus reverse transcriptase (Promega) and random hexamer primers (Amersham). Real-time qPCR was performed using SYBR Green Master Mix (Applied Biosystems) in a StepOnePlus instrument (Applied Biosystems). The primers used for qPCR are listed in Supplemental Experimental Procedures.

Mice

All mouse strains were maintained on a C57BL/6 background. Cohorts were generated by mating $p53^{+/m}$ or $p53^{+/-}$ mice. $p53^{515A}$ mice (Lang et al., 2004) harbor a G-to-A substitution at nucleotide 515, resulting in an Arg-to-His substitution at amino acid position 172 of mouse p53. Genotyping was performed by PCR analysis as described (Lang et al., 2004). Acute colitis was induced by providing 2% dextran sodium sulfate (Millipore) for 7 days in the drinking water of 8-week-old male mice weighing 21–25 g, whereas the chronic protocol involved three 5 day cycles of 2% DSS separated by 14 day intervals. Mice were monitored three times a week for overall weight, stool consistency, and gross bleeding. Colonoscopy procedures were conducted using a 1.9 mm endoscope (Karl Storz). Mice were anesthetized with 10% xylasine and 10% ketamine in PBS before colonoscopy. Inflammatory score assessment was as described in Becker et al. (2006).

Mouse organs were fixed in 4% formalin/PBS for 24 hr, embedded in paraffin, sectioned at 4 μm, dewaxed, and stained with hematoxylin and eosin. Procedures involving animals were approved by the Animal Ethics Committee of the Weizmann Institute (Institutional Animal Care and Use Committee number 05331109-2) and conformed to the guidelines of the Israel Council for Experiments in Animals. Pathological examination was conducted blindly and independently by two molecular pathologists advised by a mouse pathologist.

Human Tissues

Primary tumor and colon biopsies were obtained from the Cooperative Human Tissue Network (Office of Human Subjects Research approval number 3637) and the Mount Sinai School of Medicine. The project was approved by the institutional review boards of the National Institutes of Health and the Mount Sinai School of Medicine. Serially sectioned slides from formalin-fixed, paraffin-embedded biopsies of 18 human CAC cases were obtained from the National Cancer Institute and the Mount Sinai School of Medicine. DNA extracted from tumor cell-enriched areas of each specimen was subjected to *TP53* tagged-amplicon Illumina HiSeq 2000 sequencing (Forshew et al., 2012); K-Ras mutations were similarly interrogated. In parallel, additional slides from each specimen were subjected to immunohistochemical analysis.

Microarray Hybridization and Analysis

For expression microarray analysis, RNA was extracted as described above. RNA (10 μg) was labeled and hybridized to Affymetrix GeneChip Human Exon 1.0 ST arrays. For analysis, the Affymetrix Expression Console (parameters: annotation confidence, full; summarization method: iter-PLIER include DABG; background: PM-GCBG; normalization method: none) was used, followed by normalization of all arrays together using a Lowess multiarray algorithm. Intensity-dependent estimation of noise was used for statistical analysis of differential expression.

ACCESSION NUMBERS

The GEO accession number for the expression array data reported in this paper is GSE43738.

SUPPLEMENTAL INFORMATION

Supplemental Information includes seven figures and Supplemental Experimental Procedures and can be found with this article online at http://dx.doi.org/10.1016/j.ccr.2013.03.022.

ACKNOWLEDGMENTS

We thank Ori Brenner and Gilgi Friedlander for help with histopathological analysis and expression microarray analysis, respectively. We also thank Ronnie Apte, Elena Voronov, Derek Mann, Neil Perkins, and Yinon Ben-Neriah for helpful advice and suggestions. This work was supported in part by European Commission FP7 funding (INFLACARE agreement number 223151; INSPiRE agreement number 284460), Grant number R37 CA40099 from the National Cancer Institute, a Center of Excellence grant (1779/11) from the Israel Science Foundation, the Dr. Miriam and Sheldon Adelson Medical Research Foundation, and a Center of Excellence grant from the Flight Attendant Medical Research Institute. M.O. is the incumbent of the Andre Lwoff Chair in Molecular Biology. The European Commission is not liable for any use that may be made of the information contained herein. S.I. receives research support and is on the Scientific Advisory Board of Exact Sciences Corporation.

Received: June 15, 2012
Revised: January 17, 2013
Accepted: March 19, 2013
Published: May 13, 2013

REFERENCES

Acin, S., Li, Z., Mejia, O., Roop, D.R., El-Naggar, A.K., and Caulin, C. (2011). Gain-of-function mutant p53 but not p53 deletion promotes head and neck cancer progression in response to oncogenic K-ras. J. Pathol. *225*, 479–489.

Ak, P., and Levine, A.J. (2010). p53 and NF-κB: different strategies for responding to stress lead to a functional antagonism. FASEB J. *24*, 3643–3652.

Asquith, M., and Powrie, F. (2010). An innately dangerous balancing act: intestinal homeostasis, inflammation, and colitis-associated cancer. J. Exp. Med. *207*, 1573–1577.

Becker, C., Fantini, M.C., and Neurath, M.F. (2006). High resolution colonoscopy in live mice. Nat. Protoc. *1*, 2900–2904.

Ben-Neriah, Y., and Karin, M. (2011). Inflammation meets cancer, with NF-κB as the matchmaker. Nat. Immunol. *12*, 715–723.

Brentnall, T.A., Crispin, D.A., Rabinovitch, P.S., Haggitt, R.C., Rubin, C.E., Stevens, A.C., and Burmer, G.C. (1994). Mutations in the p53 gene: an early marker of neoplastic progression in ulcerative colitis. Gastroenterology *107*, 369–378.

Brosh, R., and Rotter, V. (2009). When mutants gain new powers: news from the mutant p53 field. Nat. Rev. Cancer *9*, 701–713.

Buganim, Y., Solomon, H., Rais, Y., Kistner, D., Nachmany, I., Brait, M., Madar, S., Goldstein, I., Kalo, E., Adam, N., et al. (2010). p53 regulates the Ras circuit to inhibit the expression of a cancer-related gene signature by various molecular pathways. Cancer Res. *70*, 2274–2284.

Campbell, I., Polyak, K., and Haviv, I. (2009). Clonal mutations in the cancer-associated fibroblasts: the case against genetic coevolution. Cancer Res. *69*, 6765–6768, discussion 6769.

Chang, W.C., Coudry, R.A., Clapper, M.L., Zhang, X., Williams, K.L., Spittle, C.S., Li, T., and Cooper, H.S. (2007). Loss of p53 enhances the induction of colitis-associated neoplasia by dextran sulfate sodium. Carcinogenesis *28*, 2375–2381.

Clapper, M.L., Cooper, H.S., and Chang, W.C. (2007). Dextran sulfate sodium-induced colitis-associated neoplasia: a promising model for the development of chemopreventive interventions. Acta Pharmacol. Sin. *28*, 1450–1459.

Dell'Orso, S., Fontemaggi, G., Stambolsky, P., Goeman, F., Voellenkle, C., Levrero, M., Strano, S., Rotter, V., Oren, M., and Blandino, G. (2011). ChIP-on-chip analysis of in vivo mutant p53 binding to selected gene promoters. OMICS *15*, 305–312.

Demaria, S., Pikarsky, E., Karin, M., Coussens, L.M., Chen, Y.C., El-Omar, E.M., Trinchieri, G., Dubinett, S.M., Mao, J.T., Szabo, E., et al. (2010). Cancer and inflammation: promise for biologic therapy. J. Immunother. *33*, 335–351.

Doyle, B., Morton, J.P., Delaney, D.W., Ridgway, R.A., Wilkins, J.A., and Sansom, O.J. (2010). p53 mutation and loss have different effects on tumourigenesis in a novel mouse model of pleomorphic rhabdomyosarcoma. J. Pathol. *222*, 129–137.

Fearon, E.R. (2011). Molecular genetics of colorectal cancer. Annu. Rev. Pathol. *6*, 479–507.

Forrester, K., Ambs, S., Lupold, S.E., Kapust, R.B., Spillare, E.A., Weinberg, W.C., Felley-Bosco, E., Wang, X.W., Geller, D.A., Tzeng, E., et al. (1996). Nitric oxide-induced p53 accumulation and regulation of inducible nitric oxide synthase expression by wild-type p53. Proc. Natl. Acad. Sci. USA *93*, 2442–2447.

Forshew, T., Murtaza, M., Parkinson, C., Gale, D., Tsui, D.W., Kaper, F., Dawson, S.J., Piskorz, A.M., Jimenez-Linan, M., Bentley, D., et al. (2012). Noninvasive identification and monitoring of cancer mutations by targeted deep sequencing of plasma DNA. Sci. Transl. Med. *4*, 136ra68.

Fujii, S., Fujimori, T., Kawamata, H., Takeda, J., Kitajima, K., Omotehara, F., Kaihara, T., Kusaka, T., Ichikawa, K., Ohkura, Y., et al. (2004). Development of colonic neoplasia in p53 deficient mice with experimental colitis induced by dextran sulphate sodium. Gut *53*, 710–716.

Geboes, K., Riddell, R., Ost, A., Jensfelt, B., Persson, T., and Löfberg, R. (2000). A reproducible grading scale for histological assessment of inflammation in ulcerative colitis. Gut *47*, 404–409.

Greten, F.R., Eckmann, L., Greten, T.F., Park, J.M., Li, Z.W., Egan, L.J., Kagnoff, M.F., and Karin, M. (2004). IKKβ links inflammation and tumorigenesis in a mouse model of colitis-associated cancer. Cell *118*, 285–296.

Guma, M., Stepniak, D., Shaked, H., Spehlmann, M.E., Shenouda, S., Cheroutre, H., Vicente-Suarez, I., Eckmann, L., Kagnoff, M.F., and Karin, M. (2011). Constitutive intestinal NF-κB does not trigger destructive inflammation unless accompanied by MAPK activation. J. Exp. Med. *208*, 1889–1900.

Hanahan, D., and Weinberg, R.A. (2011). Hallmarks of cancer: the next generation. Cell *144*, 646–674.

He, G., and Karin, M. (2011). NF-κB and STAT3—key players in liver inflammation and cancer. Cell Res. *21*, 159–168.

Hussain, S.P., Amstad, P., Raja, K., Ambs, S., Nagashima, M., Bennett, W.P., Shields, P.G., Ham, A.J., Swenberg, J.A., Marrogi, A.J., and Harris, C.C. (2000). Increased p53 mutation load in noncancerous colon tissue from ulcerative colitis: a cancer-prone chronic inflammatory disease. Cancer Res. *60*, 3333–3337.

Kinzler, K.W., and Vogelstein, B. (1996). Lessons from hereditary colorectal cancer. Cell *87*, 159–170.

Kuroda, M., Oikawa, K., Yoshida, K., Takeuchi, A., Takeuchi, M., Usui, M., Umezawa, A., and Mukai, K. (2005). Effects of 3-methylcholanthrene on the transcriptional activity and mRNA accumulation of the oncogene hWAPL. Cancer Lett. *221*, 21–28.

Lang, G.A., Iwakuma, T., Suh, Y.A., Liu, G., Rao, V.A., Parant, J.M., Valentin-Vega, Y.A., Terzian, T., Caldwell, L.C., Strong, L.C., et al. (2004). Gain of function of a p53 hot spot mutation in a mouse model of Li-Fraumeni syndrome. Cell *119*, 861–872.

Leedham, S.J., Graham, T.A., Oukrif, D., McDonald, S.A., Rodriguez-Justo, M., Harrison, R.F., Shepherd, N.A., Novelli, M.R., Jankowski, J.A., and Wright, N.A. (2009). Clonality, founder mutations, and field cancerization in human ulcerative colitis-associated neoplasia. Gastroenterology *136*, 542–550.

Levine, A.J., and Oren, M. (2009). The first 30 years of p53: growing ever more complex. Nat. Rev. Cancer *9*, 749–758.

Lozano, G. (2010). Mouse models of p53 functions. Cold Spring Harb. Perspect. Biol. *2*, a001115.

Malaterre, J., Carpinelli, M., Ernst, M., Alexander, W., Cooke, M., Sutton, S., Dworkin, S., Heath, J.K., Frampton, J., McArthur, G., et al. (2007). c-Myb is required for progenitor cell homeostasis in colonic crypts. Proc. Natl. Acad. Sci. USA *104*, 3829–3834.

Meylan, E., Dooley, A.L., Feldser, D.M., Shen, L., Turk, E., Ouyang, C., and Jacks, T. (2009). Requirement for NF-κB signalling in a mouse model of lung adenocarcinoma. Nature *462*, 104–107.

Noffsinger, A.E., Belli, J.M., Miller, M.A., and Fenoglio-Preiser, C.M. (2001). A unique basal pattern of p53 expression in ulcerative colitis is associated with mutation in the p53 gene. Histopathology *39*, 482–492.

Olive, K.P., Tuveson, D.A., Ruhe, Z.C., Yin, B., Willis, N.A., Bronson, R.T., Crowley, D., and Jacks, T. (2004). Mutant p53 gain of function in two mouse models of Li-Fraumeni syndrome. Cell *119*, 847–860.

Oren, M., and Rotter, V. (2010). Mutant p53 gain-of-function in cancer. Cold Spring Harb. Perspect. Biol. *2*, a001107.

Patocs, A., Zhang, L., Xu, Y., Weber, F., Caldes, T., Mutter, G.L., Platzer, P., and Eng, C. (2007). Breast-cancer stromal cells with TP53 mutations and nodal metastases. N. Engl. J. Med. *357*, 2543–2551.

Phelps, E.D., Updike, D.L., Bullen, E.C., Grammas, P., and Howard, E.W. (2006). Transcriptional and posttranscriptional regulation of angiopoietin-2 expression mediated by IGF and PDGF in vascular smooth muscle cells. Am. J. Physiol. Cell Physiol. *290*, C352–C361.

Rivlin, N., Brosh, R., Oren, M., and Rotter, V. (2011). Mutations in the p53 tumor suppressor gene: important milestones at the various steps of tumorigenesis. Genes Cancer *2*, 466–474.

Ryan, K.M., Ernst, M.K., Rice, N.R., and Vousden, K.H. (2000). Role of NF-κB in p53-mediated programmed cell death. Nature *404*, 892–897.

Sato, T., Vries, R.G., Snippert, H.J., van de Wetering, M., Barker, N., Stange, D.E., van Es, J.H., Abo, A., Kujala, P., Peters, P.J., and Clevers, H. (2009). Single Lgr5 stem cells build crypt-villus structures in vitro without a mesenchymal niche. Nature *459*, 262–265.

Schetter, A.J., Heegaard, N.H., and Harris, C.C. (2010). Inflammation and cancer: interweaving microRNA, free radical, cytokine and p53 pathways. Carcinogenesis *31*, 37–49.

Schneider, G., Henrich, A., Greiner, G., Wolf, V., Lovas, A., Wieczorek, M., Wagner, T., Reichardt, S., von Werder, A., Schmid, R.M., et al. (2010). Cross talk between stimulated NF-κB and the tumor suppressor p53. Oncogene *29*, 2795–2806.

Schwitalla, S., Ziegler, P.K., Horst, D., Becker, V., Kerle, I., Begus-Nahrmann, Y., Lechel, A., Rudolph, K.L., Langer, R., Slotta-Huspenina, J., et al. (2013). Loss of p53 in enterocytes generates an inflammatory microenvironment enabling invasion and lymph node metastasis of carcinogen-induced colorectal tumors. Cancer Cell *23*, 93–106.

Scian, M.J., Stagliano, K.E., Anderson, M.A., Hassan, S., Bowman, M., Miles, M.F., Deb, S.P., and Deb, S. (2005). Tumor-derived p53 mutants induce NF-κB2 gene expression. Mol. Cell. Biol. *25*, 10097–10110.

Shema, E., Tirosh, I., Aylon, Y., Huang, J., Ye, C., Moskovits, N., Raver-Shapira, N., Minsky, N., Pirngruber, J., Tarcic, G., et al. (2008). The histone H2B-specific ubiquitin ligase RNF20/hBRE1 acts as a putative tumor suppressor through selective regulation of gene expression. Genes Dev. *22*, 2664–2676.

Suh, Y.A., Post, S.M., Elizondo-Fraire, A.C., Maccio, D.R., Jackson, J.G., El-Naggar, A.K., Van Pelt, C.S., Terzian, T., and Lozano, G. (2011). Multiple stress signals activate mutant p53 in vivo. Cancer Res. *71*, 7168–7175.

Sur, S., Pagliarini, R., Bunz, F., Rago, C., Diaz, L.A., Jr., Kinzler, K.W., Vogelstein, B., and Papadopoulos, N. (2009). A panel of isogenic human cancer cells suggests a therapeutic approach for cancers with inactivated p53. Proc. Natl. Acad. Sci. USA *106*, 3964–3969.

Tanaka, T., Kohno, H., Suzuki, R., Yamada, Y., Sugie, S., and Mori, H. (2003). A novel inflammation-related mouse colon carcinogenesis model induced by azoxymethane and dextran sodium sulfate. Cancer Sci. *94*, 965–973.

Tergaonkar, V., and Perkins, N.D. (2007). p53 and NF-κB crosstalk: IKKα tips the balance. Mol. Cell *26*, 158–159.

Terzian, T., Suh, Y.A., Iwakuma, T., Post, S.M., Neumann, M., Lang, G.A., Van Pelt, C.S., and Lozano, G. (2008). The inherent instability of mutant p53 is alleviated by Mdm2 or p16INK4a loss. Genes Dev. *22*, 1337–1344.

Terzic, J., Grivennikov, S., Karin, E., and Karin, M. (2010). Inflammation and colon cancer. Gastroenterology *138*, 2101–2114.

Ullman, T.A., and Itzkowitz, S.H. (2011). Intestinal inflammation and cancer. Gastroenterology *140*, 1807–1816.

Vlantis, K., Wullaert, A., Sasaki, Y., Schmidt-Supprian, M., Rajewsky, K., Roskams, T., and Pasparakis, M. (2011). Constitutive IKK2 activation in intestinal epithelial cells induces intestinal tumors in mice. J. Clin. Invest. *121*, 2781–2793.

Vousden, K.H., and Prives, C. (2009). Blinded by the light: the growing complexity of p53. Cell *137*, 413–431.

Weisz, L., Damalas, A., Liontos, M., Karakaidos, P., Fontemaggi, G., Maor-Aloni, R., Kalis, M., Levrero, M., Strano, S., Gorgoulis, V.G., et al. (2007). Mutant p53 enhances nuclear factor κB activation by tumor necrosis factor α in cancer cells. Cancer Res. *67*, 2396–2401.

Wernert, N., Löcherbach, C., Wellmann, A., Behrens, P., and Hügel, A. (2001). Presence of genetic alterations in microdissected stroma of human colon and breast cancers. Anticancer Res. *21*, 2259–2264.

Yin, J., Harpaz, N., Tong, Y., Huang, Y., Laurin, J., Greenwald, B.D., Hontanosas, M., Newkirk, C., and Meltzer, S.J. (1993). p53 point mutations in dysplastic and cancerous ulcerative colitis lesions. Gastroenterology *104*, 1633–1639.

Yoshida, T., Mikami, T., Mitomi, H., and Okayasu, I. (2003). Diverse p53 alterations in ulcerative colitis-associated low-grade dysplasia: full-length gene sequencing in microdissected single crypts. J. Pathol. *199*, 166–175.